Condensation heat transfer on superhydrophobic surfaces

Condensation Heat Transfer on Superhydrophobic Surfaces

Nenad Miljkovic and Evelyn N. Wang*

Department of Mechanical Engineering, Massachusetts Institute of Technology,
77 Massachusetts Avenue, Cambridge, Massachusetts 02139, USA

*Address correspondence to enwang@mit.edu

Abstract (150 words max)

Condensation is a phase change phenomenon often encountered in nature and industry for applications including power generation, thermal management, desalination, and environmental control. For the past eight decades, researchers have focused on creating surfaces allowing condensed droplets to be easily removed by gravity for enhanced heat transfer performance. Recent advancements in nanofabrication have enabled increased control of surface structuring for the development of superhydrophobic surfaces with even higher droplet mobility, and in some cases, coalescence-induced droplet jumping. Here, we provide a review of new insights gained to tailor superhydrophobic surfaces for enhanced condensation heat transfer considering the role of surface structure, nucleation density, droplet morphology, and droplet dynamics. Furthermore, we identify challenges and new opportunities to advance these surfaces for broad implementation into thermo-fluidic systems.

Keywords: superhydrophobic surface, condensation heat transfer, dropwise condensation, condensation modeling, nanostructures, jumping droplets

Introduction

Vapor condensation is a ubiquitous phenomenon occurring in nature[1-5]. We observe this process in our daily lives, such as on a hot summer day when water accumulates on a cold drink or when fog forms on a humid day. In industry, vapor condensation is an essential process in power generation[6], thermal management[7], water desalination[8,9], and environmental control[10]. For example, the thermal efficiency of the steam cycle, responsible for the majority of an industrialized nation's power production, is directly linked to condensation heat transfer performance. Meanwhile, in heating, ventilating, and air conditioning (HVAC) systems, which account for ≈20% of the total energy consumption in developed countries[11], the accumulation of condensed water on thermal components can lead to performance degradation and increased costs. Furthermore, condensation on glass strongly influences the transmittance of light into greenhouses, resulting in possible losses of 40% during the winter[12].

In these systems, vapor condenses on a surface rather than directly in the vapor phase due to the reduced energy barrier for droplet nucleation[13]. However, the vapor typically forms a thin liquid film because of the high surface energy of industrial components (*i.e.*, clean metals such as copper, aluminum, stainless steel). While this mode which is known as filmwise condensation[14] (Figure 1a) is quite common, the formation of a liquid film is not desired due to the large resistance to heat transfer. Meanwhile, if a surface is coated with a low-energy non-wetting 'promoter' material (*i.e.*, long chain fatty acid, wax, polymer coating, self-assembled monolayer)[15-19], or if it naturally adsorbs hydrocarbons and impurities on its surface from the surroundings (as in the case of gold, silver, and chromium)[20-22], the vapor forms discrete liquid droplets ranging in size from microns to millimeters[23-25]. This process is known as dropwise condensation[26] (Figure 1b). The progressive removal of these condensing droplets by gravity at length scales comparable to the capillary length (≈2.7 mm for water)[27-29] helps refresh the surface for re-nucleation, and allows 5 – 7*x* higher heat transfer performance when compared to the filmwise mode[30].

For the past eight decades, dropwise condensation on common heat transfer materials has been a topic of significant interest[30,31], with a focus on creating non-wetting surfaces *via* promoter coatings for easy droplet removal. While robust coatings still continue to be a challenge and require more development[30], recent advancements in nanofabrication have allowed for the development of superhydrophobic surfaces[32], where nearly spherical water droplets form

with high mobility and minimal droplet adhesion. In addition, the role of surface structuring on wetting characteristics have been studied in detail[33-35] to enhance condensation performance by reducing droplet departure sizes ($\lesssim$ 3 mm) and enabling faster clearing of the surface for re-nucleation.

Yet when small water droplets (≈10−100 μm) merge on suitably designed superhydrophobic surfaces, they can undergo coalescence-induced droplet ejection or "jumping" due to the release of excess surface energy (Figure 1c) [29]. Jumping droplet condensation has offered a new avenue to further enhance heat transfer by increasing the time-averaged density of small droplets. However if the nucleation density is too high and the spacing between droplets is reduced, droplet jumping cannot be sustained. Under such conditions, discrete droplets highly adhered to the surface form and can have even worse performance than dropwise condensation, leading to a flooding condensation mode (Figure 1d). The different fluid-surface interactions of the four modes described above (filmwise, dropwise, jumping, and flooding) accordingly determine the heat transfer performance.

To characterize the condensation performance, the heat flux, q" is a commonly used metric to quantify the amount of latent heat of phase change removed by the surface at a given driving potential. This driving potential is represented by either the vapor–surface temperature difference ($\Delta T = T_{sat}(P_v) - T_{wall}$) or the supersaturation, S, the ratio of the vapor pressure to the saturation pressure at the surface temperature, $S = p_{vap} / p_{sat}(T_{wall})$. Accordingly, Figure 1e summarizes the measured (filmwise and dropwise) and expected (jumping and flooding) performance of the four modes, showing q" with ΔT for steam at atmospheric pressure[30]. If the condensing steam is mixed with non-condensable gases, NCGs (air), the NCG can accumulate adjacent to the surface creating an additional diffusional resistance for vapor molecules. The high sensitivity of condensation heat transfer to small amounts (< 10 ppm) of air in the steam explains the large range of values and trends shown in Figure 1e for the case of dropwise condensation with NCGs. With the development of superhydrophobic materials, the heat transfer performance should theoretically be able to exceed that of the highest values reported with dropwise condensation. However, due to the complex fluid-surface interactions, the role of structures for enhanced condensation on superhydrophobic surfaces has been unclear until recently, where we have gained new understanding on fluid-surface processes during phase change.

In this article, we review the fabrication, characterization, wettability, and interfacial dynamics of superhydrophobic materials during condensation and discuss insights from recent studies for enhanced heat transfer performance. The review focuses on water as the working fluid due to its favorable heat transfer properties (*i.e.*, high latent heat of vaporization) and its common use in industry. To better understand the physics of the process, we examine the role of structures on emerging droplet morphology, nucleation density, droplet growth rate, and departure characteristics. Furthermore, we discuss scalable materials for superhydrophobic surfaces with experimentally demonstrated heat transfer performance. Finally, we provide perspectives for the development of next generation nanostructured materials for enhanced condensation heat transfer.

Condensation Physics on Superhydrophobic Surfaces

Wetting Phenomena

We first briefly provide background related to wetting phenomena to facilitate understanding of condensation on superhydrophobic surfaces.

When a droplet is deposited on a flat surface, it can either wet the surface or form a discrete droplet depending on the surface energy. Young[36] first proposed that the equilibrium contact angle, θ, of the droplet is dictated by a force balance at the three phase contact line:

$$\cos\theta = \frac{\gamma_{sv} - \gamma_{sl}}{\gamma_{lv}}, \tag{1}$$

where γ_{sv}, γ_{sl} and γ_{lv} are the solid-vapor, solid-liquid, and liquid-vapor surface tensions, respectively. Continuing the work of Young, Wenzel and Cassie subsequently extended the wetting analysis to rough and porous surfaces. Considering a surface with roughness, r, defined by the ratio of the total surface area to the projected area, Wenzel[37] showed when the fluid wets all of the rough area, the contact angle θ_W is defined by:

$$\cos\theta_W = r\cos\theta\,. \tag{2}$$

In contrast, Cassie and Baxter[38] considered the case where the droplet rests on the tips of the roughness and showed that the contact angle θ_C is defined by:

$$\cos\theta_C = \varphi\,(\cos\theta + 1) - 1\,, \tag{3}$$

where φ is the ratio of the solid area contacting the droplet to the projected area. The two droplet morphologies described by equations 2 and 3 are termed Wenzel and Cassie, respectively. Accordingly, in the case of hydrophobic surfaces ($\theta > 90^{\circ}$), the roughness amplifies the wetting characteristics such that the surface becomes superhydrophobic, where contact angles exceed 150˚. While Wenzel and Cassie droplets can both exist on these rough surfaces, the Wenzel state is less desired owing to the higher adhesion to the substrate compared to the low adhesion Cassie state[32]. As a result, over the past decade, studies have focused on developing superhydrophobic surfaces to limit droplet adhesion and increase water repellency[32,39-43].

In the case of condensation, however, the nucleation of droplets through the vapor phase can initiate within the roughness, such that Equations 2 and 3 may not apply. Previous studies have shown that on structured superhydrophobic surfaces with well-controlled geometries (defined in Figure 2a), highly adhered Wenzel droplets form during vapor condensation, which are distinct from the highly mobile Cassie droplets when deposited using a syringe[32,44-46]. In fact, three different droplet morphologies exist during condensation, Wenzel (W) (Figures 2a, d), partially wetting (PW) (Figures 2b, e), and suspended (S) (Figures 2c, f), where both S and PW droplets are highly mobile compared to W droplets. Due to the importance of minimizing droplet adhesion, knowledge of the emergent droplet morphology needs to be properly characterized and understood in order to tailor the micro/nanostructured surfaces with controlled roughness, *i.e.*, surface structuring, for enhanced heat transfer[47].

Structure Geometry and Nucleation Density

Structure geometry and nucleation density have specific roles in the emergent droplet morphology (PW, S, or W). Previous studies have shown that there is a length-scale dependency of the surface structuring, *i.e.*, microstructures[45,48,49] versus nanostructures[29,50-53], and that global thermodynamic analysis comparing the lower equilibrium energy state, *i.e.*, Cassie vs Wenzel, is insufficient[40], while often used to explain observed condensation behavior[45,46,48,49,54]. Recently, Enright et al. showed that the morphology of isolated droplets interacting with the surface structures during growth from within a unit cell (volume between structures) is primarily due to: 1) energy barriers encountered by the droplet growing within the structured surface (Figure 3a), and 2) droplet-droplet interactions governed by the nucleation density, *i.e.*, the average spacing between nucleation sites $\langle L \rangle$ relative to the structure length scale l.[55] Meanwhile, S droplets

nucleating on the tips of structures are unconditionally stable assuming no droplet-droplet interactions and external forces such as gravity.

Enright *et al.* focused on droplets nucleating within the unit cell because they are more desirable for enhanced heat transfer. Their study showed that these droplets can either grow above the structure forming a 'balloon' like PW droplet (Figure 3b), or laterally spread into the structure forming a highly adhered W droplet (Figure 3c)[54,55]. While the droplet morphology is dictated by the intricate liquid/structure interaction dynamics, it can be approximately predicted by comparing the energies of the *non-equilibrium* advancing Cassie and Wenzel states with a dimensionless energy ratio:

$$E^* = \frac{\cos\theta_{a,C}}{\cos\theta_{a,W}} = \frac{-1}{r\cos\theta_a}, \quad (4)$$

where $r = 1 + \pi dh/l^2$ is the surface roughness, and θ_a is the advancing contact angle on a flat surface. Equation 4 implies that when $E^* > 1$, W droplet morphologies are favored, while when $E^* < 1$, PW droplets should emerge[55]. In addition to this energy criterion, the nuclei of the droplets need to be 2-5*x* of the spacing between the structures (Figure 3d) ($\langle L\rangle/l > 2-5$). If droplets grow and merge too close to each other such that $\langle L\rangle/l < 2-5$, coalescence events bypass the energy barrier associated with individual droplet growth (Equation 4) and flood the surface forming undesired highly adhered W droplets (Figure 3e). Accordingly, a regime map defining the parametric space with experimentally measured $\langle L\rangle/l$ ratios and calculated E^* in Figure 3f determines the emergent droplet morphology for a wide variety of structure length scales, geometries and nucleation densities. The results suggest that an important aspect is defining the location of, and distance between nucleation sites to favor formation of highly mobile PW droplet morphologies.

Tailoring Surface Chemistry for Nucleation

Controlling nucleation has been investigated, but has primarily focused on patterning surface chemistry heterogeneities[56-62] (hybrid hydrophobic/hydrophilic surfaces) at the length scale of the structures or larger to simultaneously increase the nucleation rate (hydrophilic spots) and achieve high droplet mobility (hydrophobic spots). Although spatial control of nucleation has been demonstrated[58], it was also accompanied by higher droplet adhesion[63]. The hydrophilic spots on the surface act to pin the droplet and result in slower removal[30]. However, S droplets

with low adhesion were obtained using hybrid surfaces by ensuring that the height to thickness ratio of the structures (*i.e.*, with pillars having hydrophilic tops and hydrophobic valleys) is relatively large[63]. Therefore, with proper design, hybrid surfaces have the potential to enhance droplet shedding for enhanced condensation while controlling nucleation density.

To define the location of nucleation sites at length scales smaller than the structure (< 10 nm), in order to delay flooding condensation, Enright et al.[55] showed that defects in the hydrophobic coatings exist[64-66], which with the proper structure geometry can be used to determine the formation of highly mobile PW and S droplets. Hydrophobic coatings with tailored defects present an opportunity to control droplet morphology while further enhancing heat transfer.

Effect of Droplet Morphology on Growth Dynamics

While both PW and S droplets show advantages in terms of easy droplet removal as opposed to W droplets, droplet growth prior to departure needs to be considered to determine the desired morphology for enhanced heat transfer. Miljkovic et al.[67] highlighted the importance of considering droplet morphology on growth rates whereby in certain cases, surface structuring can degrade heat transfer performance. Using a specific structure geometry, they demonstrated that the growth rate and individual droplet heat transfer of PW droplets were 6*x* and 4-6*x* higher than that of S droplets, respectively (Figure 4a, b). This difference was due to the fact that S droplets are suspended on top of a composite air-solid interface, where the air is a significant thermal resistance to droplet growth. To investigate the effect of the morphology on overall surface heat transfer, a thermal resistance based droplet growth model was developed[67-71] (Figure 4c) and demonstrated that surfaces favoring only S droplet formation degraded overall performance by 71% when compared to flat hydrophobic shedding surfaces, despite their high mobility[67]. The study showed structure design needs to be carefully considered to minimize the effect of the air beneath the droplet, while maintaining easy droplet removal. Accordingly, this thermal resistance can be decreased by reducing the structure heights *via* nanoscale roughness.

To tailor the emergent droplet morphology, Miljkovic at al.[47] suggested a method to favor PW droplet formation *via* the creation of thermodynamic energy barriers for nucleation on structure tips[72]. By making the tip thickness comparable to the critical nucleation radius (≈10-30 nm for water), the energy barrier for nucleation on the tip is increased, resulting in favorable

droplet nucleation within the structure and stable formation of PW droplets[47]. It is important to note, this approach is valid assuming the nucleation density of droplets is low compared to the density of the structures ($\langle L \rangle / l > 2-5$) such that flooding is avoided (Figure 3f).

Droplet Departure

Once the droplets nucleate and grow with the desired morphology, droplets also need to be quickly removed from the surface to enhance heat transfer[73]. The recent works of Boreyko et al.[29] and Narhe et al.[74] presented a new experimental approach for efficient droplet departure, whereby condensate droplets spontaneously jump on a superhydrophobic surface without any external forces (Figure 5b). The average droplet radius at steady-state was thirty times smaller than the capillary length (≈2.7 mm for water), and therefore promises significant heat transfer improvement due to the smaller time averaged distribution of droplets[75]. The spontaneous motion is powered by the surface energy released upon droplet coalescence and the out-of-plane jumping results from in-plane coalescence (Figure 5c,d). While both PW and S droplet morphologies are capable of jumping at equivalent length scales[76], as discussed earlier PW droplets are favored due to their higher growth rates[67]. It is important to note, if the solid fraction of the structure is too large ($\varphi \geq 0.1$), PW and S droplet jumping may not be possible due to high adhesion.

To achieve droplet jumping, surface structures need to be designed with minimal droplet adhesion by using nanoscale structures with low solid fractions ($\varphi \geq 0.1$), or hierarchical structures[77-81] (consisting of a dual length scale roughness of micro and nano structure). Extending the work of Boreyko, many researchers have modeled[76,82-84] and fabricated[50,52,85-89] surfaces that show stable droplet jumping. However, if the supersaturation is too large (high nucleation density), flooding occurs and droplets strongly adhered to the surface are formed[47,55]. These nucleation density limitations still remain and need to be addressed to further increase the operating range of superhydrophobic surfaces. Furthermore, heat transfer measurements are required to better quantify the condensation enhancement when compared to state-of-the-art dropwise condensing surfaces.

Condensation Heat Transfer Performance on Superhydrophobic Surfaces

Modeling of Enhanced Superhydrophobic Surfaces

As shown by the previous studies, condensation heat transfer performance on superhydrophobic surfaces is dependent on many factors including droplet morphology, structure geometry, and departure dynamics. To obtain design guidelines for enhanced condensation heat transfer with superhydrophobic structured surfaces, Miljkovic et al.[84] developed a unified model coupling individual droplet heat transfer, droplet size distribution, and droplet wetting morphology. The emergent droplet wetting morphologies, PW and S jumping, PW and S non-jumping, or W, were determined by coupling the structure geometry with the nucleation density and considering local energy barriers to wetting. The model results suggest that a specific range of geometries (0.5 – 2 μm) and nucleation densities, allow for the formation of coalescence-induced PW jumping droplets with a promise of 190% overall surface heat flux enhancement over conventional flat dropwise condensing surfaces[84].

Fabrication of Scalable Nanostructures

While a considerable amount of work has focused on understanding and fabricating superhydrophobic surfaces for potential enhancements in condensation[29,52,54,67,68,74,75,86-90], heat transfer measurements that quantify the improvement in performance using these surfaces are limited. In addition, many studies have used well-defined structures to facilitate the understanding of the condensation process (carbon nanotubes[53], nanowires[54], and nanoparticle self-assembly[91], micropillars[55,58]), however, it is also important to pursue scalable methods of fabricating superhydrophobic surfaces for the implementation in large scale thermal applications.

Recently, researchers have proposed metal oxides to fabricate more scalable superhydrophobic nanostructured surfaces[47,85,86,92-96]. The nanoscale oxide can 1) better satisfy the requirement for the structure density to be larger than the nucleation density in order to avoid flooding[55], and 2) reduce the structure length scale beneath the droplet in order to minimize the structure thermal resistance[67].

The works of Miljkovic et al.[47] (Figure 6a-c), Feng et al.[85,94], and Torresin et al.[93] (Figure 6d-f) studied scalable functionalized copper oxide (CuO) nanostructured surfaces. Copper is a typical heat exchanger material where chemical-oxidation based CuO nanostructuring allows for a self-limiting growth behavior, resulting in a low characteristic oxide

thickness ($h \approx 1$ μm) and a low parasitic conduction thermal resistance[97,98]. From an industrial perspective, the CuO fabrication method is appealing because it can be applied to arbitrarily shaped surfaces, where the nanostructures form at low temperatures and do not require any high temperature annealing or drying processes. While zinc oxide (ZnO) has also been proposed, Narhe et al.[92] showed that the ZnO nanostructures had favorable morphology (Figure 6g-i), but were not able to achieve droplet jumping due to incomplete hydrophobic coating coverage, relatively large solid fractions $\varphi \approx 0.11$, and subsequently larger droplet adhesion to the surface.

Furthermore, in addition to copper and zinc, opportunities remain to create scalable nanostructured superhydrophobic surfaces with aluminum and stainless steel, which are commonly used industrial heat exchanger materials[30].

Heat Transfer Experiments

An important metric for optimized superhydrophobic surfaces for condensation are experimental heat transfer measurements, however, it is well-known that accurate results are difficult to obtain. Due to the high sensitivity to the presence of non-condensable gasses (NCGs), experiments need to be performed in controlled environments to ensure NCG content of $< 0.25\%$.[30,99] In addition, the interfacial resistances, *i.e.*, thermal grease, between the sample substrate and test rig have led to a lack of repeatability in heat transfer measurements. Recently, a few studies have conducted experimental investigations in pure vapor environments (no NCGs)[47,93,100,101]. The first performance measurement was achieved by Boreyko et al.[100] *via* the characterization of a jumping droplet thermal diode (Figure 7a). Although indirect (condensation and evaporation performance were lumped together), the results showed forward and reverse effective thermal conductivities of 350 W/mK and 0.29 W/mK, respectively (Figure 7b), indicating that the jumping droplet mechanism enhanced heat transfer.

To specifically quantify condensation heat transfer performance, Miljkovic et al.[47] tested superhydrophobic nanostructured CuO surfaces over a range of supersaturations ($1.02 < S < 1.6$) (Figure 7c). They demonstrated that in the jumping regime where $S < 1.12$, heat transfer coefficients were $h_{jumping} \approx 92$ kW/m^{2}K, 30% higher than that of state-of-the-art dropwise condensing copper surfaces. However, at $S > 1.12$, flooding degraded performance to $h_{flooded} \approx 44$kW/m^{2}K, 41% less than that of copper. Other studies have also observed flooding on two-tier superhydrophobic CNT[101] and nanostructured CuO[93] surfaces, due to high nucleation

densities compared to the structure density (Figure 3f), consequently underperforming compared to dropwise condensation.

Although the results show potential for efficient droplet jumping heat transfer enhancement, the flooding observed by many researchers suggests the needed to further reduce the structure length scale and/or reduce and control the nucleation density at elevated supersaturations.

Summary and Future Outlook

Superhydrophobic surfaces for enhanced condensation requires the careful control of surface structure length scale and geometry, nucleation density, droplet morphology, and departure dynamics. Currently, metal oxides are one of the most promising methods to create these superhydrophobic surfaces in a scalable manner due to their ability to form PW droplets, relatively large thermal conductivities, reduced structure length scales, and low droplet adhesion for stable droplet jumping. In addition, jumping condensation has the potential to enhance heat transfer in the presence of NCGs[102-104] *via* boundary layer mixing, in addition to the 30% enhancement already observed in pure vapor environments. However, these surfaces remain limited due to flooding for applications with low supersaturations. In the future, control of nucleation density through the creation of coatings and deposition methods for the inclusion of well-defined defects at the molecular scale, and minimization of the structure length scale are promising pathways to extend the operating limits. Furthermore, significant efforts should be placed on creating robust hydrophobic coatings at high temperatures. As in classical dropwise condensation, the degradation of the hydrophobic coating poses significant challenges for industrial implementation. One idea showing promise is the study and formation of naturally occurring hydrophobic materials, such as rare-earth oxide ceramics[105].

A second avenue for future research is with structured surfaces infused with a lubricating fluid, *i.e.*, SLIPS, to reduce droplet adhesion[106,107]. SLIPS provide an alternative approach for further performance enhancement at larger supersaturations[108], eliminating flooding of the surface structure while maintaining low droplet adhesion[109-112]. In addition, the ability of these surfaces to be omniphobic[113-116] or superamphiphobic allows for their potential use in applications involving low surface tension non-polar fluids such as refrigerants, where superhydrophobic surfaces can no longer achieve non-wetting behavior. Although promising,

further studies into the robustness of SLIPS under industrial conditions, as well as their longevity, are needed in addition to experimental demonstration of heat transfer performance. While limitations exist, progress in the area of superhydrophobic surfaces for enhanced heat transfer has been considerable, deepening our fundamental knowledge, introducing new scalable fabrication techniques, and setting new benchmarks for heat transfer performance. Further advances in creating and tailoring robust nanostructures and hydrophobic coatings promise to one day make superhydrophobic surfaces the material of choice for high heat flux condensation applications.

Acknowledgements

We gratefully acknowledge funding support from the MIT S3TEC Center, an Energy Frontier Research Center funded by the Department of Energy, Office of Science, Office of Basic Energy Sciences, Office of Naval Research Young Investigator Award, and Air Force Office of Scientific Research Young Investigator Award.

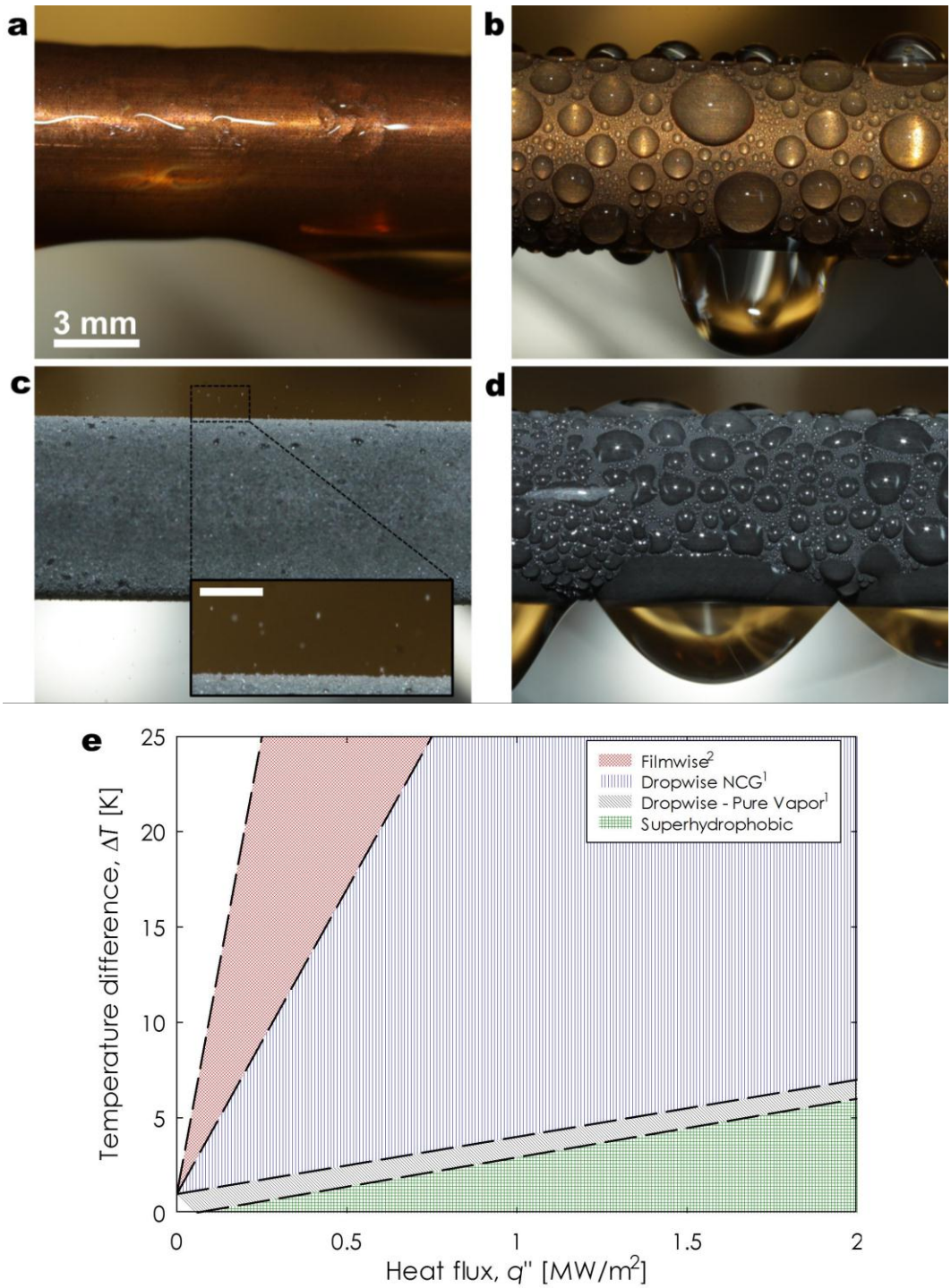

Figure 1 – Condensation heat transfer modes and performance. Images of (a) filmwise condensation on a smooth hydrophilic Cu tube, (b) dropwise condensation on a silane coated smooth Cu tube, (c) jumping-droplet superhydrophobic condensation on a nanostructured CuO tube (Inset: magnified view of the jumping phenomena, scale bar is 500 μm), and (d) flooding condensation on a nanostructured CuO tube[47]. (e) Heat transfer measurements for dropwise condensation of steam at near-atmospheric pressure[30] ($\Delta T = T_{sat}(P_v) - T_{wall}$). Superhydrophobic region shows expected performance enhancement due to increased droplet mobility. Reprinted with permission from reference 47. Copyright 2013, American Chemical Society.

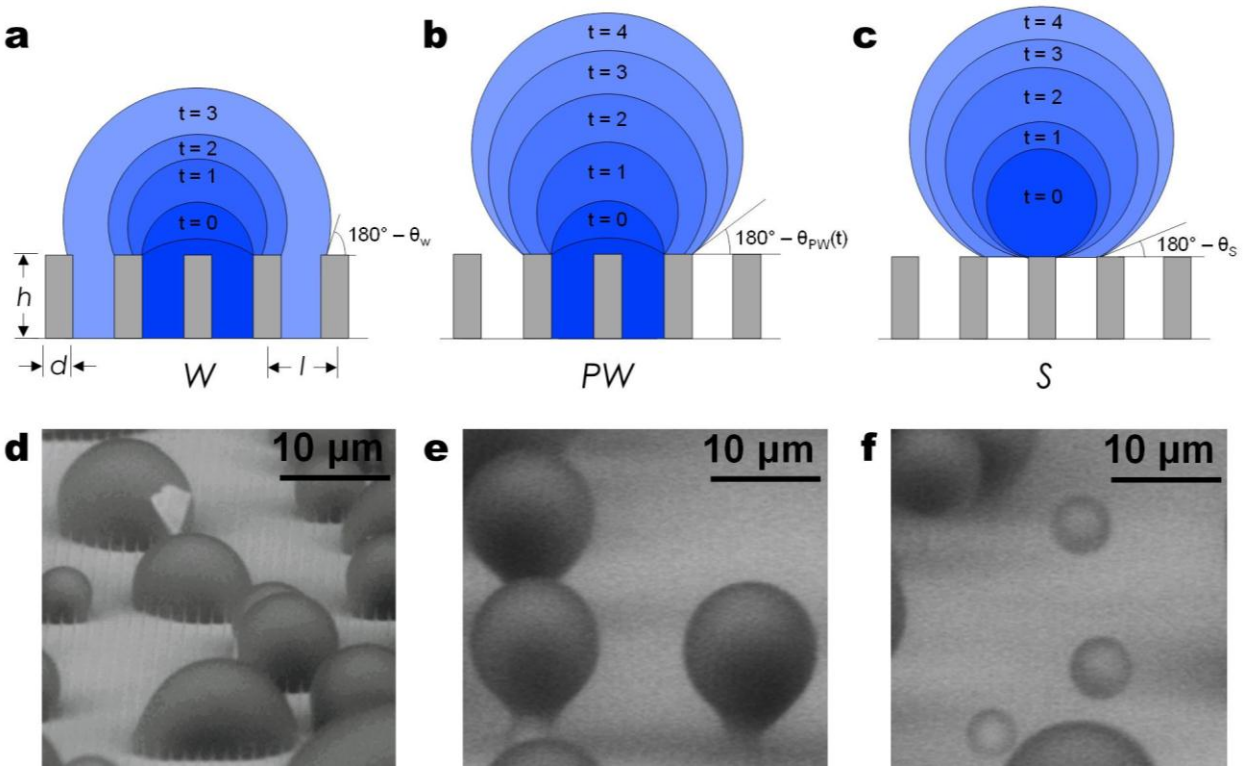

Figure 2 – Condensing droplet morphologies. Time-lapse schematics of a (a) Wenzel (W) droplet where liquid fills the structures beneath the droplet; (b) partially wetting (PW) droplet where the liquid partially fills the structure beneath the droplet, and (c) suspended (S) droplet where an air layer fills the structure beneath the droplet[84] (schematics not to scale). Environmental scanning electron microscopy (ESEM)[117-127] images of droplets with the (d) W, (e) PW, and (f) S morphologies on a nanostructured surface (h = 6.1 µm, l = 2 µm, d = 300 nm)[67].Reprinted with permission from reference 84. Copyright 2013, American Society of Mechanical Engineers.

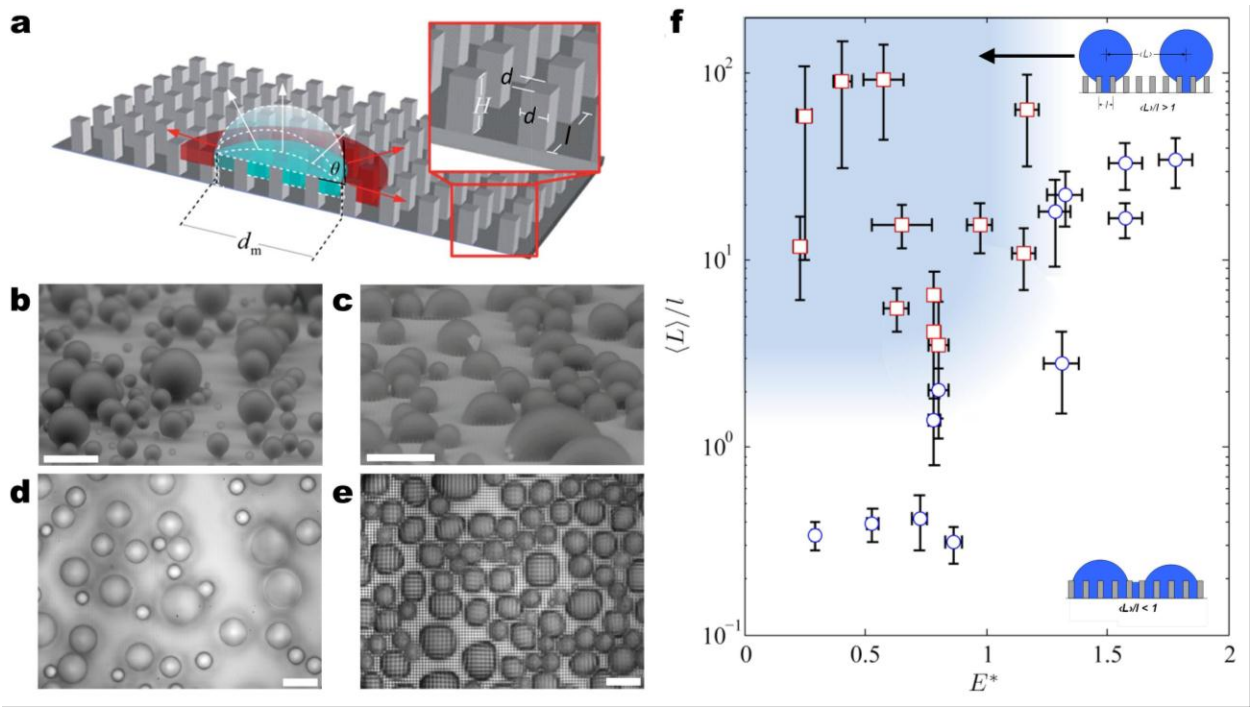

Figure 3 – Effect of structure length scale and nucleation density on emergent droplet morphology. (a) Schematic of a droplet growing within the confines of the structures. The liquid can either grow laterally by filling the adjacent structures or by growing upwards above the structures[54]. Condensed droplet growth observed using ESEM on structured surfaces with (b) Cassie droplets where $l = 2$ μm and (c) Wenzel droplets where $l = 4$ μm.[55] Scale bar for (b, c) is 60 μm. Condensation behavior on a microstructured surface ($l = 4.5$ μm, $d = 2$ μm, $h = 5$ μm, and $E^* = 0.75 \pm 0.04$) is shown at a fixed location with a scaled coalescence length of (d) $\langle L \rangle / l = 3.54 \pm 2.43$ (PW droplets) and (e) $\langle L \rangle / l = 2.04 \pm 0.6$ (W droplets)[55]. Scale bar for (d, e) is 50 μm. (f) Regime map characterizing the dominant wetting behavior observed during condensation with coordinates of $\langle L \rangle / l$ and E^*. PW morphologies (red □) emerge at large $\langle L \rangle / l$ and $E^* \lesssim 1$ (shaded region). Wenzel morphologies (blue ○) emerge at low $\langle L \rangle / l$ and/or $E^* \gtrsim 1$.[55] Adapted with permission from references 55 (Copyright 2013, American Chemical Society) and 54 (Copyright 2012, Royal Society of Chemistry).

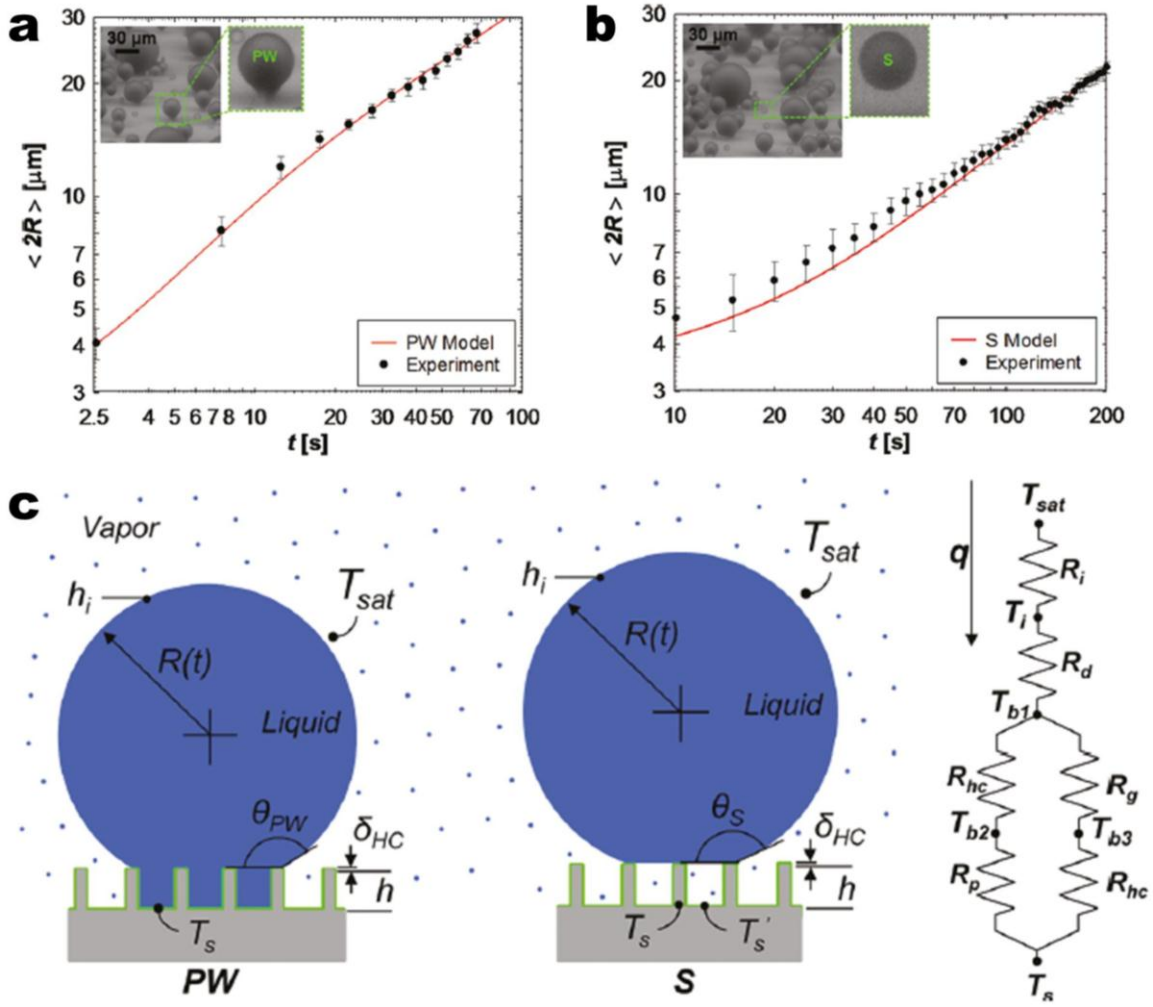

Figure 4 – Effect of droplet morphology on growth rate. Time evolution of the average droplet diameter for (a) PW and (b) S droplets. The S droplet has a slower growth rate than the PW droplet due to poor thermal contact between the base and substrate[67]. (c) PW and S droplet model schematics and thermal resistance diagram showing the liquid-vapor interface (R_i), droplet conduction (R_d), hydrophobic coating (R_{hc}), pillar (R_p), and gap (R_g) thermal resistances[67]. Reprinted with permission from references 67. Copyright 2012, American Chemical Society.

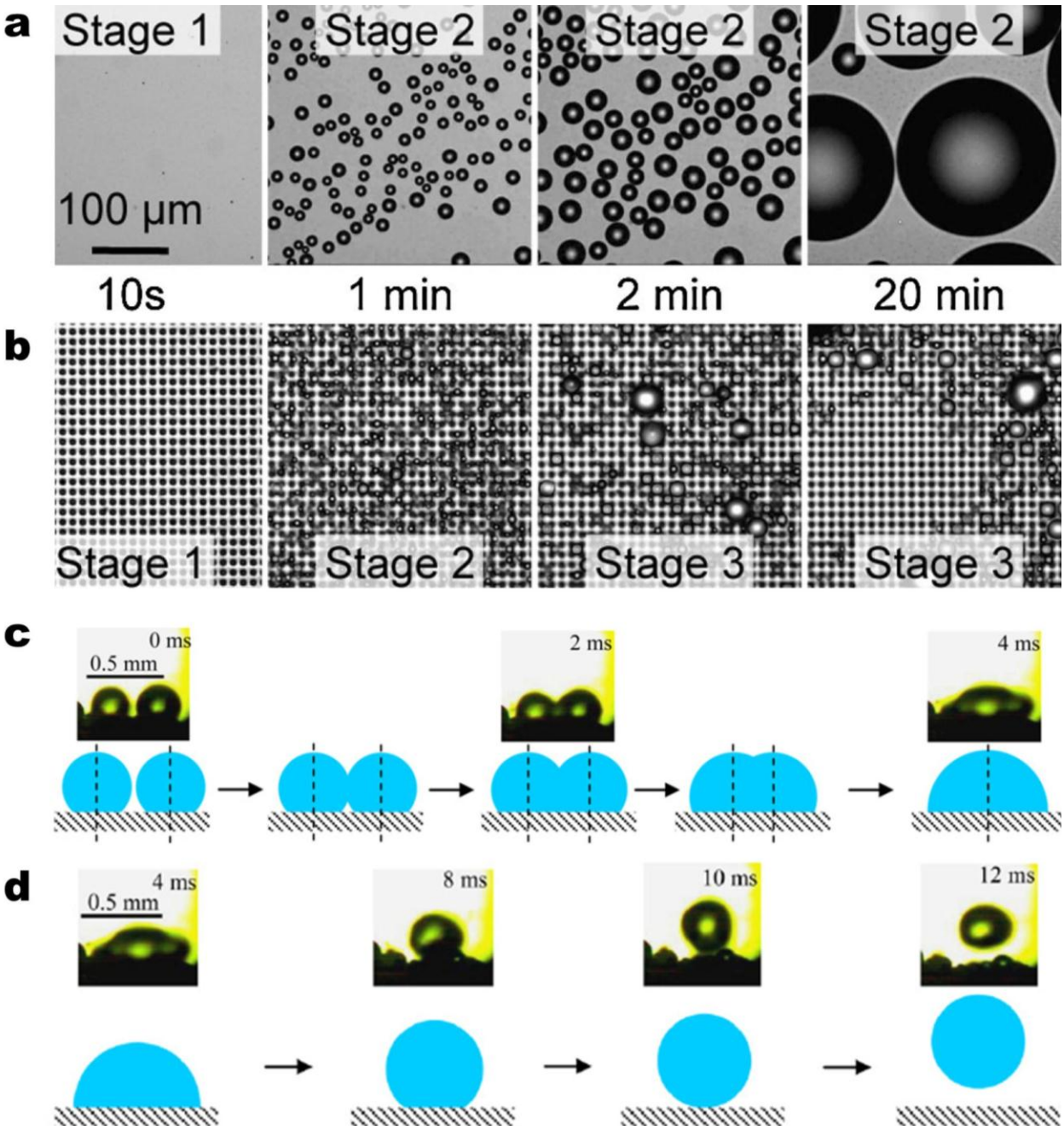

Figure 5 – Droplet departure modes – gravitational shedding versus jumping. Dropwise condensation on a horizontally oriented (a) smooth hydrophobic surface and (b) structured two-tier superhydrophobic surface (with micro pillars visible). Stages 1–3 of the condensation process characterize the initial nucleation, immobile coalescence, and mobile coalescence (jumping droplets), respectively[29]. (c) Coalescing process of two droplets. Upper photos: side-view imaging of two condensed drops with diameters of 302 and 252 μm during merging; lower: modeled coalescence process[83]. (d) Coalescence-induced transformation and jumping of the merged droplet. Upper photos: side-view images of coalescence-induced droplet jumping; lower: modeled coalescence-induced droplet jumping[83]. Reprinted with permission from references 29 (Copyright 2009, The American Physical Society) and 83 (Copyright 2012, Elsevier).

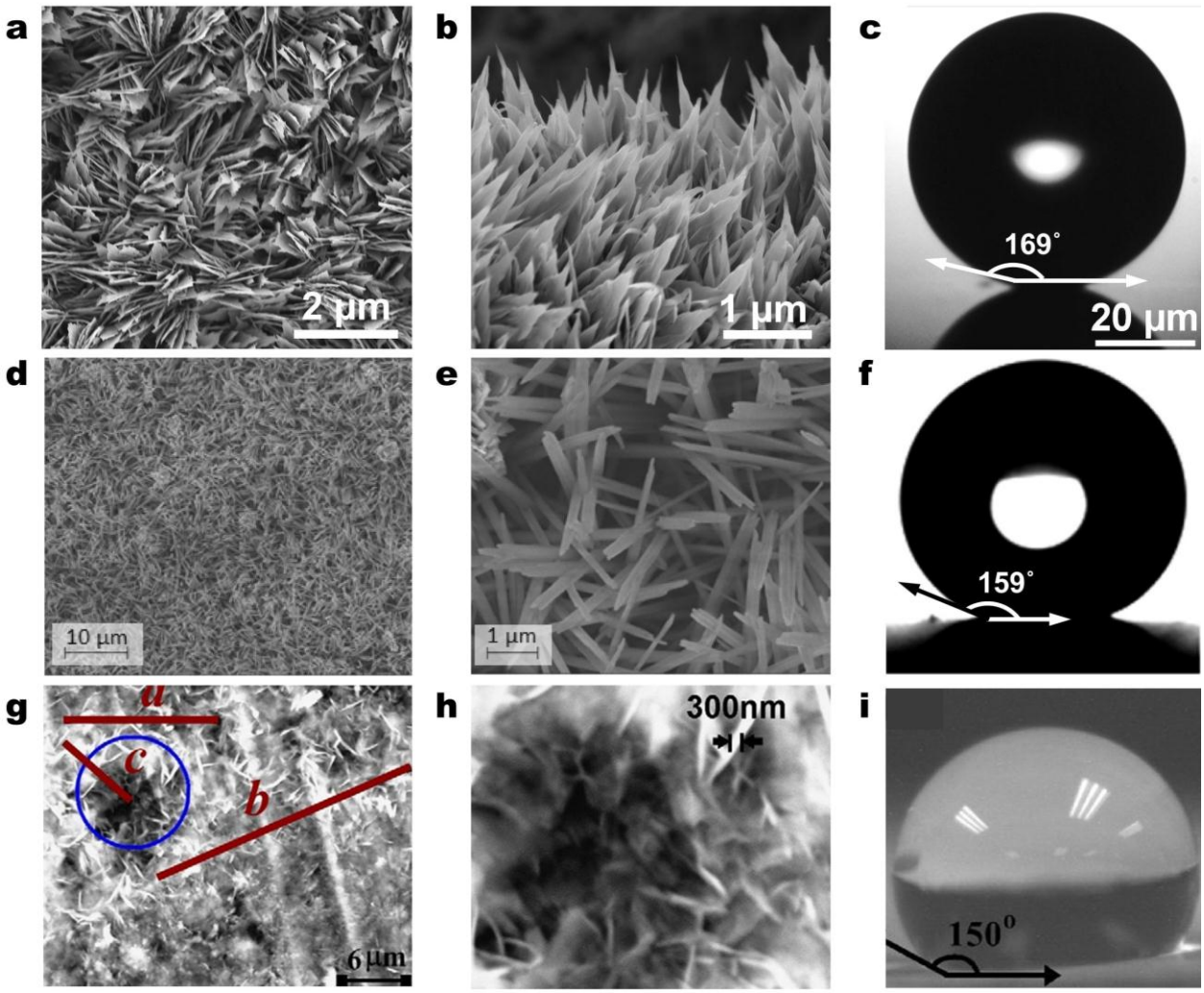

Figure 6 – Fabricated scalable nanostructured surfaces. FESEM images of a 5 min CuO surface with (a) top view, (b) side view, and (c) micro-goniometer contact angle measurement image ($\theta_a = 169.2 \pm 2.6^o$). The sharp, knife-like CuO structures have characteristic heights, $h \approx 1$ µm, solid fraction, $\varphi \approx 0.023$, and roughness factor, $r \approx 10$.[47] (d, e) SEM images of the copper surface structures at a 12 min immersion time[93]. (f) Contact angle measurement on the nanostructured superhydrophobic copper surface (5 µL droplet, $\theta_a = 159 \pm 2^o$)[93]. (g) SEM images of zinc surface (24 h deposition) showing micro-flowers-like structure ($a \approx 12$ µm, $b \approx 25$ µm, $c \approx 10$ µm)[92]. (h) The micro-flower area inside the circle in (g) at large magnification. It shows nano sheets with average thickness 300 nm[92]. (i) Contact angle measurement of a 3 µl water droplet on the ZnO surface. Reprinted with permission from references 47, 93 (Copyright 2013, American Chemical Society), and 92 (Copyright 2010, Elsevier).

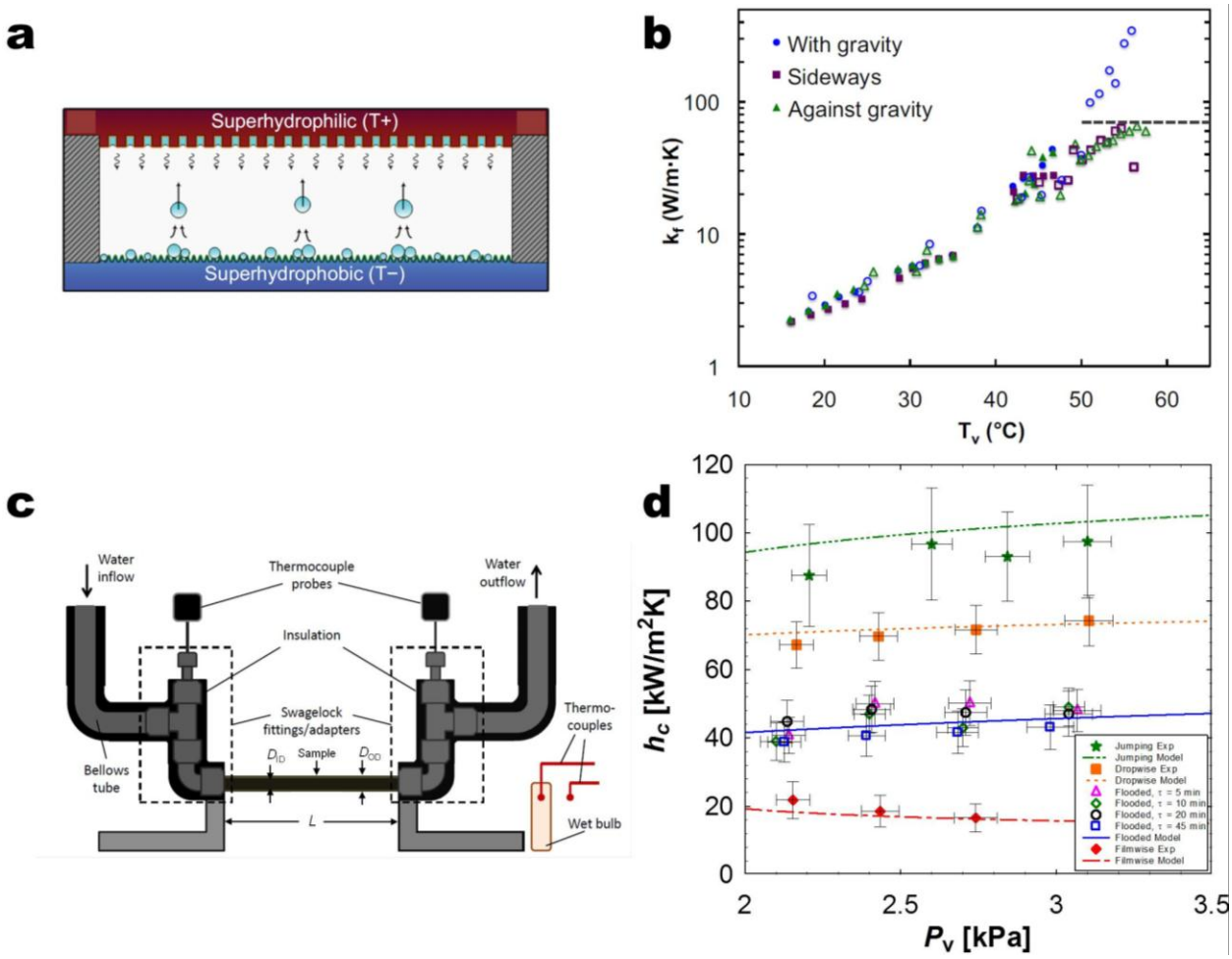

Figure 7 – Experimental heat transfer results. (a) Schematic of the planar jumping-droplet thermal diode (not to scale) in forward mode with jumping droplets returning the working fluid from the superhydrophobic condenser to the superhydrophilic evaporator for continuous phase-change heat transfer[100]. (b) Forward thermal conductivity (k_f) versus the average vapor temperature of the thermal diode (T_v).[100] (c) Schematic showing experimental setup. The tube sample (D_{OD} = 6.35 mm, D_{ID} = 3.56 mm, L = 131 mm) was cooled *via* chilled water flowing inside the tube at 5 ± 0.1 L/min[47]. (h) Experimental and theoretical steady state condensation coefficient (h_c) as a function of saturated vapor pressure (P_v) for tube surfaces shown in (d) undergoing filmwise, dropwise, flooding (τ = 5, 10, 20, and 45 min), and jumping (τ = 10 min) condensation[47]. Jumping condensation shows the highest condensation HTC for low supersaturations (S < 1.12).[47] Adapted with permission from references 100 (Copyright 2012, American Institute of Physics), and 47 (Copyright 2013, American Chemical Society).

References

1 Parker, A. R. & Lawrence, C. R. Water capture by a desert beetle. *Nature* **414**, 33-34, (2001).

2 Zheng, Y. M. *et al.* Directional water collection on wetted spider silk. *Nature* **463**, 640-643, (2010).

3 Bhushan, B. Biomimetics: lessons from nature - an overview. *Philos T R Soc A* **367**, 1445-1486, (2009).

4 Cheng, Y. T. & Rodak, D. E. Is the lotus leaf superhydrophobic? *Appl Phys Lett* **86**, (2005).

5 Mockenhaupt, B., Ensikat, H. J., Spaeth, M. & Barthlott, W. Superhydrophobicity of Biological and Technical Surfaces under Moisture Condensation: Stability in Relation to Surface Structure. *Langmuir* **24**, 13591-13597, (2008).

6 Beer, J. M. High efficiency electric power generation: The environmental role. *Prog Energ Combust* **33**, 107-134, (2007).

7 Peters, T. B. *et al.* Design of an Integrated Loop Heat Pipe Air-Cooled Heat Exchanger for High Performance Electronics. *Ieee T Comp Pack Man* **2**, 1637-1648, (2012).

8 Khawaji, A. D., Kutubkhanah, I. K. & Wie, J. M. Advances in seawater desalination technologies. *Desalination* **221**, 47-69, (2008).

9 Humplik, T. *et al.* Nanostructured materials for water desalination. *Nanotechnology* **22**, (2011).

10 Perez-Lombard, L., Ortiz, J. & Pout, C. A review on buildings energy consumption information. *Energ Buildings* **40**, 394-398, (2008).

11 Li, B. Z. & Yao, R. M. Urbanisation and its impact on building energy consumption and efficiency in China. *Renew Energ* **34**, 1994-1998, (2009).

12 von Elsner, B. *et al.* Review of structural and functional characteristics of greenhouses in European Union countries: Part I, Design requirements. *J Agr Eng Res* **75**, 1-16, (2000).

13 Kaschiev, D. *Nucleation: Basic Theory With Applications*. (Butterworth Heinemann, 2000).

14 Nusselt, W. Z. Die Oberfliichenkondensation des Wasserdampfes. *Z. Ver. Deut. Ing.* **60**, 541-546, (1916).

15 Marto, P. J., Looney, D. J., Rose, J. W. & Wanniarachchi, A. S. Evaluation of Organic Coatings for the Promotion of Dropwise Condensation of Steam. *Int J Heat Mass Tran* **29**, 1109-1117, (1986).

16 Bonner, R. W. I. in *Proceedings of the International Heat Transfer Conference* (ASME, Washington, DC, USA, 2010).

17 Vemuri, S., Kim, K. J., Wood, B. D., Govindaraju, S. & Bell, T. W. Long term testing for dropwise condensation using self-assembled monolayer coatings of n-octadecyl mercaptan. *Appl Therm Eng* **26**, 421-429, (2006).

18 Vemuri, S. & Kim, K. J. An experimental and theoretical study on the concept of dropwise condensation. *Int J Heat Mass Tran* **49**, 649-657, (2006).

19 Das, A. K., Kilty, H. P., Marto, P. J., Andeen, G. B. & Kumar, A. The use of an organic self-assembled monolayer coating to promote dropwise condensation of steam on horizontal tubes. *J Heat Trans-T Asme* **122**, 278-286, (2000).

20 Erb, R. A. & Thelen, E. Promoting Permanent Dropwise Condensation. *Ind Eng Chem* **57**, 49-&, (1965).

21 Wilkins, D. G., Bromley, L. A. & Read, S. M. Dropwise and Filmwise Condensation of Water Vapor on Gold. *Aiche J* **19**, 119-123, (1973).
22 Woodruff, D. W. & Westwater, J. W. Steam Condensation on Electroplated Gold - Effect of Plating Thickness. *Int J Heat Mass Tran* **22**, 629-632, (1979).
23 Beysens, D. Dew Nucleation and Growth. *Cr Phys* **7**, 1082-1100, (2006).
24 Beysens, D., Steyer, A., Guenoun, P., Fritter, D. & Knobler, C. M. How Does Dew Form. *Phase Transit* **31**, 219-246, (1991).
25 Fritter, D., Knobler, C. M. & Beysens, D. A. Experiments and Simulation of The Growth of Droplets on a Surface (Breath Figures). *Phys Rev A* **43**, 2858-2869, (1991).
26 Schmidt, E., Schurig, W. & Sellschopp, W. Versuche über die Kondensation von Wasserdampf in Film- und Tropfenform. *Forsch. Ingenieurwes* **1**, 53–63, (1930).
27 Kim, H. Y., Lee, H. J. & Kang, B. H. Sliding of Liquid Drops Down an Inclined Solid Surface. *J Colloid Interf Sci* **247**, 372-380, (2002).
28 Dimitrakopoulos, P. & Higdon, J. J. L. On The Gravitational Displacement of Three-Dimensional Fluid Droplets From Inclined Solid Surfaces. *J Fluid Mech* **395**, 181-209, (1999).
29 Boreyko, J. B. & Chen, C. H. Self-Propelled Dropwise Condensate on Superhydrophobic Surfaces. *Phys Rev Lett* **103**, 184501-184501 - 184501-184504, (2009).
30 Rose, J. W. Dropwise condensation theory and experiment: a review. *P I Mech Eng a-J Pow* **216**, 115-128, (2002).
31 Sikarwar, B. S., Khandekar, S., Agrawal, S., Kumar, S. & Muralidhar, K. Dropwise Condensation Studies on Multiple Scales. *Heat Transfer Eng* **33**, 301-341, (2012).
32 Lafuma, A. & Quere, D. Superhydrophobic States. *Nature Materials* **2**, 457-460, (2003).
33 Patankar, N. A. Supernucleating surfaces for nucleate boiling and dropwise condensation heat transfer. *Soft Matter* **6**, 1613-1620, (2010).
34 Bocquet, L. & Lauga, E. A smooth future? *Nature Materials* **10**, 334-337, (2011).
35 Kang, S. H., Wu, N., Grinthal, A. & Aizenberg, J. Meniscus Lithography: Evaporation-Induced Self-Organization of Pillar Arrays into Moire Patterns. *Phys Rev Lett* **107**, 177802-177801 - 177802-177805, (2011).
36 Young, T. An Essay on the Cohesion of Fluids. *Phil. Trans. R. Soc. Lond.* **95**, 65–87, (1805).
37 Wenzel, R. N. Resistance of Solid Surfaces to Wetting by Water. *Ind. Eng. Chem.* **28**, 988-994, (1936).
38 Cassie, A. B. D. & Baxter, S. Wettability of Porous Surfaces *Trans. Faraday Soc* **40** 546-551, (1944).
39 Gao, L. C., Fadeev, A. Y. & McCarthy, T. J. Superhydrophobicity and contact-line issues. *Mrs Bull* **33**, 747-751, (2008).
40 Quere, D. Wetting and roughness. *Annu Rev Mater Res* **38**, 71-99, (2008).
41 Dorrer, C. & Ruhe, J. Some thoughts on superhydrophobic wetting. *Soft Matter* **5**, 51-61, (2009).
42 Roach, P., Shirtcliffe, N. J. & Newton, M. I. Progess in superhydrophobic surface development. *Soft Matter* **4**, 224-240, (2008).
43 Moulinet, S. & Bartolo, D. Life and Death of a Fakir Droplet: Impalement Transitions on Superhydrophobic Surfaces. *Eur Phys J E* **24**, 251-260, (2007).
44 Narhe, R. D. & Beysens, D. A. Water Condensation on a Super-Hydrophobic Spike Surface. *Europhys Lett* **75**, 98-104, (2006).

45 Narhe, R. D. & Beysens, D. A. Nucleation and Growth on a Superhydrophobic Grooved Surface. *Phys Rev Lett* **93**, 076103-076101 - 076103-076104, (2004).
46 Narhe, R. D. & Beysens, D. A. Growth dynamics of water drops on a square-pattern rough hydrophobic surface. *Langmuir* **23**, 6486-6489, (2007).
47 Miljkovic, N. *et al.* Jumping-Droplet-Enhanced Condensation on Scalable Superhydrophobic Nanostructured Surfaces. *Nano Lett* **13**, 179-187, (2013).
48 Dorrer, C. & Ruhe, J. Condensation and wetting transitions on microstructured ultrahydrophobic surfaces. *Langmuir* **23**, 3820-3824, (2007).
49 Wier, K. A. & McCarthy, T. J. Condensation on ultrahydrophobic surfaces and its effect on droplet mobility: Ultrahydrophobic surfaces are not always water repellant. *Langmuir* **22**, 2433-2436, (2006).
50 Chen, C. H. *et al.* Dropwise Condensation on Superhydrophobic Surfaces With Two-Tier Roughness. *Appl Phys Lett* **90**, 173108-173101 - 173108-173103, (2007).
51 Dorrer, C. & Ruhe, J. Wetting of silicon nanograss: From superhydrophilic to superhydrophobic surfaces. *Adv Mater* **20**, 159-+, (2008).
52 Chen, X. *et al.* Nanograssed Micropyramidal Architectures for Continuous Dropwise Condensation. *Adv Funct Mater* **21**, 4617–4623, (2011).
53 Lau, K. K. S. *et al.* Superhydrophobic Carbon Nanotube Forests. *Nano Lett* **3**, 1701-1705, (2003).
54 Rykaczewski, K. *et al.* How nanorough is rough enough to make a surface superhydrophobic during water condensation? *Soft Matter* **8**, 8786-8794, (2012).
55 Enright, R., Miljkovic, N., Al-Obeidi, A., Thompson, C. V. & Wang, E. N. Superhydrophobic Condensation: The Role of Length Scale and Energy Barriers. *Langmuir* **40**, 14424–14432, (2012).
56 Anderson, D. M. *et al.* Using Amphiphilic Nanostructures To Enable Long-Range Ensemble Coalescence and Surface Rejuvenation in Dropwise Condensation. *Acs Nano* **6**, 3262-3268, (2012).
57 Varanasi, K. K. & Deng, T. in *12th Ieee Intersociety Conference on Thermal and Thermomechanical Phenomena in Electronic Systems* 1-5 (Los Vegas, NV, 2010).
58 Varanasi, K. K., Hsu, M., Bhate, N., Yang, W. S. & Deng, T. Spatial Control in the Heterogeneous Nucleation of Water. *Appl Phys Lett* **95**, 094101-094101 - 094101-094103, (2009).
59 Her, E. K., Ko, T. J., Lee, K. R., Oh, K. H. & Moon, M. W. Bioinspired steel surfaces with extreme wettability contrast. *Nanoscale* **4**, 2900-2905, (2012).
60 Ji, S. M. *et al.* Fabrication of a Hybrid Superhydrophobic/superhydrophilic Surface for Water Collection: Gravure Offset Printing & Colloidal Lithography. *Journal of the Korean Society of Precision Engineering* **29**, 19-24, (2012).
61 Lee, A., Moon, M. W., Lim, H., Kim, W. D. & Kim, H. Y. Water harvest via dewing. *Langmuir* **28**, 10183-10191, (2012).
62 Thickett, S. C., Neto, C. & Harris, A. T. Biomimetic Surface Coatings for Atmospheric Water Capture Prepared by Dewetting of Polymer Films. *Adv Mater* **23**, 3718-+, (2011).
63 Yao, C. W. *et al.* Droplet contact angle behavior on a hybrid surface with hydrophobic and hydrophilic properties. *Appl Phys Lett* **101**, (2012).
64 Love, J. C., Estroff, L. A., Kriebel, J. K., Nuzzo, R. G. & Whitesides, G. M. Self-assembled monolayers of thiolates on metals as a form of nanotechnology. *Chem Rev* **105**, 1103-1169, (2005).

65 Lopez, G. P., Biebuyck, H. A., Frisbie, C. D. & Whitesides, G. M. Imaging of Features on Surfaces by Condensation Figures. *Science* **260**, 647-649, (1993).
66 Mandler, D. & Turyan, I. Applications of self-assembled monolayers in electroanalytical chemistry. *Electroanal* **8**, 207-213, (1996).
67 Miljkovic, N., Enright, R. & Wang, E. N. Effect of Droplet Morphology on Growth Dynamics and Heat Transfer during Condensation on Superhydrophobic Nanostructured Surfaces. *Acs Nano* **6**, 1776–1785, (2012).
68 Rykaczewski, K. Microdroplet Growth Mechanism during Water Condensation on Superhydrophobic Surfaces. *Langmuir* **28**, 7720-7729, (2012).
69 Kim, S. & Kim, K. J. Dropwise Condensation Modeling Suitable for Superhydrophobic Surfaces. *J Heat Transf* **133**, 081502-081501 - 081502-081507, (2011).
70 AbuOrabi, M. Modeling of Heat Transfer in Dropwise Condensation. *Int J Heat Mass Tran* **41**, 81-87, (1998).
71 Anand, S. & Son, S. Y. Sub-Micrometer Dropwise Condensation Under Superheated and Rarefied Vapor Condition. *Langmuir* **26**, 17100-17110, (2010).
72 Cao, L. L., Jones, A. K., Sikka, V. K., Wu, J. Z. & Gao, D. Anti-Icing Superhydrophobic Coatings. *Langmuir* **25**, 12444-12448, (2009).
73 Rose, J. W. & Glicksman, L. R. Dropwise condensation - the distribution of drop sizes. *Int J Heat Mass Tran* **16**, 411-425, (1973).
74 Narhe, R. D., Khandkar, M. D., Shelke, P. B., Limaye, A. V. & Beysens, D. A. Condensation-Induced Jumping Water Drops. *Phys Rev E* **80**, 031604-031601 - 031604-031605, (2009).
75 Dietz, C., Rykaczewski, K., Fedorov, A. G. & Joshi, Y. Visualization of Droplet Departure on a Superhydrophobic Surface and Implications to Heat Transfer Enhancement During Dropwise Condensation. *Appl Phys Lett* **97**, 033104-033101 - 033104-033103, (2010).
76 Miljkovic, N., Enright, R. & Wang, E. N. Growth Dynamics During Dropwise Condensation on Nanostructured Superhydrophobic Surfaces. *3rd Micro/Nanoscale Heat & Mass Transfer International Conference*, (2012).
77 Nosonovsky, M. & Bhushan, B. Hierarchical roughness optimization for biomimetic superhydrophobic surfaces. *Ultramicroscopy* **107**, 969-979, (2007).
78 McCarthy, M. *et al.* Biotemplated hierarchical surfaces and the role of dual length scales on the repellency of impacting droplets. *Appl Phys Lett* **100**, 1-5, (2012).
79 Bhushan, B. & Nosonovsky, M. Biomimetic Superhydrophobic Surfaces: Multiscale Approach. *Nano Lett* **7**, 2633-2637, (2007).
80 Bhushan, B. & Jung, Y. C. Mechanically Durable Carbon Nanotube-Composite Hierarchical Structures with Superhydrophobicity, Self-Cleaning, and Low-Drag. *Acs Nano* **3**, 4155-4163, (2009).
81 Pokroy, B., Kang, S. H., Mahadevan, L. & Aizenberg, J. Self-Organization of a Mesoscale Bristle into Ordered, Hierarchical Helical Assemblies. *Science* **323**, 237-240, (2009).
82 Liu, T. Q., Sun, W., Sun, X. Y. & Ai, H. R. Thermodynamic Analysis of the Effect of the Hierarchical Architecture of a Superhydrophobic Surface on a Condensed Drop State. *Langmuir* **26**, 14835-14841, (2010).
83 Liu, T. Q., Sun, W., Sun, X. Y. & Ai, H. R. Mechanism study of condensed drops jumping on super-hydrophobic surfaces. *Colloid Surface A* **414**, 366-374, (2012).

84 Miljkovic, N., Enright, R. & Wang, E. N. Modeling and Optimization of Condensation Heat Transfer on Micro and Nanostructured Superhydrophobic Surfaces. *J Heat Transf* **in press**, (2012).
85 Feng, J., Pang, Y., Qin, Z., Ma, R. & Yao, S. Why Condensate Drops Can Spontaneously Move Away on Some Superhydrophobic Surfaces but Not on Others. *ACS Applied Materials & Interfaces* **4**, 6618−6625, (2012).
86 Enright, R., Dou, N., Miljkovic, N., Nam, Y. & Wang, E. N. Condensation on Superhydrophobic Copper Oxide Nanostructures. *3rd Micro/Nanoscale Heat & Mass Transfer International Conference*, (2012).
87 Dietz, C., Rykaczewski, K., Fedorov, A. & Joshi, Y. ESEM Imaging of Condensation on a Nanostructured Superhydrophobic Surface. *J Heat Trans-T Asme* **132**, 080904-080901, (2010).
88 Boreyko, J. B. & Collier, P. C. Delayed Frost Growth on Jumping-Drop Superhydrophobic Surfaces. *Acs Nano*, (2013).
89 Rykaczewski, K. *et al.* Three Dimensional Aspects of Droplet Coalescence During Dropwise Condensation on Superhydrophobic Surfaces. *Soft Matter* **7**, 8749-8752, (2011).
90 Rykaczewski, K. *et al.* Multimode Multidrop Serial Coalescence Effects during Condensation on Hierarchical Superhydrophobic Surfaces. *Langmuir* **29**, 881–891, (2013).
91 Rykaczewski, K. *et al.* Dynamics of Nanoparticle Self-Assembly into Superhydrophobic Liquid Marbles During Water Condensation. *Acs Nano* **5**, 9746–9754, (2011).
92 Narhe, R. D., Gonzalez-Vinas, W. & Beysens, D. A. Water Condensation on Zinc Surfaces Treated by Chemical Bath Deposition. *Appl Surf Sci* **256**, 4930-4933, (2010).
93 Torresin, D., Tiwari, M. K., Del Col, D. & Poulikakos, D. Flow Condensation on Copper-Based Nanotextured Superhydrophobic Surfaces. *Langmuir* **29**, 840−848, (2013).
94 Feng, J., Qin, Z. Q. & Yao, S. H. Factors Affecting the Spontaneous Motion of Condensate Drops on Superhydrophobic Copper Surfaces. *Langmuir* **28**, 6067-6075, (2012).
95 Zhang, X. T. *et al.* Preparation and photocatalytic wettability conversion of TiO2-based superhydrophobic surfaces. *Langmuir* **22**, 9477-9479, (2006).
96 Zhang, X. T. *et al.* Superhydrophobic TiO2 surfaces: Preparation, photocatalytic wettability conversion, and superhydrophobic-superhydrophilic patterning. *J Phys Chem C* **111**, 14521-14529, (2007).
97 Nam, Y., Sharratt, S., Byon, C., Kim, S. J. & Ju, Y. S. Fabrication and Characterization of the Capillary Performance of Superhydrophilic Cu Micropost Arrays. *Journal of Microelectromechanical Systems* **19**, 581 - 588 (2010).
98 Nam, Y. & Sungtaek, Y. A comparative study of the morphology and wetting characteristics of micro/nanostructured Cu surfaces for phase change heat transfer applications. *Journal of Adhesion Science and Technology*, 1-14, (2012).
99 Rose, J. W. On the Mechanism of Dropwise Condensation. *Int J Heat Mass Tran* **10**, 755-762, (1967).
100 Boreyko, J. B., Zhao, Y. J. & Chen, C. H. Planar jumping-drop thermal diodes. *Appl Phys Lett* **99**, (2011).

101 Cheng, J., Vandadi, A. & Chen, C. L. Condensation heat transfer on two-tier superhydrophobic surfaces. *Appl Phys Lett* **101**, 131909-131901 - 131909-131904, (2012).

102 Ma, X. H., Zhou, X. D., Lan, Z., Li, Y. M. & Zhang, Y. Condensation Heat Transfer Enhancement in the Presence of Non-Condensable Gas Using the Interfacial Effect of Dropwise Condensation. *Int J Heat Mass Tran* **51**, 1728-1737, (2008).

103 Rose, J. W. Approximate equation for forced convection in thepresence of non-condensable gas on flat plate and horizontal tube. *Int J Heat Mass Tran* **23**, 539-546, (1980).

104 Thiel, G. P. & Lienhard, J. H. Entropy generation in condensation in the presence of high concentrations of noncondensable gases. *Int J Heat Mass Tran* **55**, 5133-5147, (2012).

105 Azimi, G., Dhiman, R., Kwon, H. K., Paxson, A. T. & Varanasi, K. K. Hydrophobicity of rare-earth oxide ceramics. *Nature Materials*, (2013).

106 Lafuma, A. & Quere, D. Slippery pre-suffused surfaces. *Epl-Europhys Lett* **96**, (2011).

107 Wong, T. S. *et al.* Bioinspired self-repairing slippery surfaces with pressure-stable omniphobicity. *Nature* **477**, 443-447, (2011).

108 Anand, S., Paxson, A. T., Dhiman, R., Smith, D. J. & Varanasi, K. K. Enhanced Condensation on Lubricant-Impregnated Nanotextured Surfaces *Acs Nano* **6**, 10122–10129, (2012).

109 Kim, P. *et al.* Liquid-Infused Nanostructured Surfaces with Extreme Anti-Ice and Anti-Frost Performance. *Acs Nano* **6**, 6569-6577, (2012).

110 Wilson, P. W. *et al.* Inhibition of ice nucleation by slippery liquid-infused porous surfaces (SLIPS). *Phys. Chem. Chem. Phys.* **15**, 581--585, (2013).

111 Epstein, A. K., Wong, T. S., Belisle, R. A., Boggs, E. M. & Aizenberg, J. Liquid-infused structured surfaces with exceptional anti-biofouling performance. *P Natl Acad Sci USA* **109**, 13182-13187, (2012).

112 Smith, D. J. *et al.* Droplet mobility on lubricant-impregnated surfaces. *Soft Matter* **9**, 1772-1780, (2013).

113 Tuteja, A., Choi, W. J., McKinley, G. H., Cohen, R. E. & Rubner, M. F. Design parameters for superhydrophobicity and superoleophobicity. *Mrs Bull* **33**, 752-758, (2008).

114 Deng, X., Mammen, L., Butt, H. J. & Vollmer, D. Candle Soot as a Template for a Transparent Robust Superamphiphobic Coating. *Science* **335**, 67-70, (2012).

115 Nishimoto, S. & Bhushan, B. Bioinspired self-cleaning surfaces with superhydrophobicity, superoleophobicity, and superhydrophilicity. *Rsc Adv* **3**, 671-690, (2013).

116 Liu, X. J., Liang, Y. M., Zhou, F. & Liu, W. M. Extreme wettability and tunable adhesion: biomimicking beyond nature? *Soft Matter* **8**, 2070-2086, (2012).

117 Stokes, D. & Royal Microscopical Society (Great Britain). *Principles and practice of variable pressure/environmental scanning electron microscopy (VP-ESEM).* (Wiley, 2008).

118 Stelmashenko, N. A., Craven, J. P., Donald, A. M., Terentjev, E. M. & Thiel, B. L. Topographic contrast of partially wetting water droplets in environmental scanning electron microscopy. *J Microsc-Oxford* **204**, 172-183, (2001).

119 Rossi, M. P., Gogotsi, Y. & Kornev, K. G. Deformation of Carbon Nanotubes by Exposure to Water Vapor. *Langmuir* **25**, 2804-2810, (2009).

120 Miljkovic, N., Enright, R., Maroo, S. C., Cho, H. J. & Wang, E. N. Liquid Evaporation on Superhydrophobic and Superhydrophilic Nanostructured Surfaces. *J Heat Transf* **133**, 080903-080901, (2011).
121 Miljkovic, N., Enright, R. & Wang, E. N. Liquid Freezing Dynamics on Hydrophobic and Superhydrophobic Surfaces. *J Heat Trans-T Asme* **134**, (2012).
122 Barkay, Z. Wettability study using transmitted electrons in environmental scanning electron microscope. *Appl Phys Lett* **96**, (2010).
123 Bhushan, B. & Jung, Y. C. Wetting Behaviour During Evaporation and Condensation of Water Microdroplets on Superhydrophobic Patterned Surfaces. *J Microsc-Oxford* **229**, 127-140, (2008).
124 Rykaczewski, K. & Scott, J. H. J. Methodology for Imaging Nano-to-Microscale Water Condensation Dynamics on Complex Nanostructures. *Acs Nano* **5**, 5962-5968, (2011).
125 Rykaczewski, K., Scott, J. H. J. & Fedorov, A. G. Electron Beam Heating Effects During Environmental Scanning Electron Microscopy Imaging of Water Condensation on Superhydrophobic Surfaces. *Appl Phys Lett* **98**, 093106-093101 - 093106-093103, (2011).
126 Wiedemann, S., Plettl, A., Walther, P. & Ziemann, P. Freeze Fracture Approach to Directly Visualize Wetting Transitions on Nanopatterned Superhydrophobic Silicon Surfaces: More than a Proof of Principle. *Langmuir* **29**, 913-919, (2013).
127 Rykaczewski, K., Landin, T., Walker, M. L., Scott, J. H. J. & Varanasi, K. K. Direct Imaging of Complex Nano- to Microscale Interfaces Involving Solid, Liquid, and Gas Phases. *Acs Nano* **6**, 9326-9334, (2012).

Figure Captions

Figure 1 – Condensation heat transfer modes and performance. Images of (a) filmwise condensation on a smooth hydrophilic Cu tube, (b) dropwise condensation on a silane coated smooth Cu tube, (c) jumping-droplet superhydrophobic condensation on a nanostructured CuO tube (Inset: magnified view of the jumping phenomena, scale bar is 500 μm), and (d) flooding condensation on a nanostructured CuO tube[47]. (e) Heat transfer measurements for dropwise condensation of steam at near-atmospheric pressure[30] ($\Delta T = T_{sat}(P_v) - T_{wall}$). Superhydrophobic region shows expected performance enhancement due to increased droplet mobility. Reprinted with permission from reference 47. Copyright 2013, American Chemical Society.

Figure 2 – Condensing droplet morphologies. Time-lapse schematics of a (a) Wenzel (W) droplet where liquid fills the structures beneath the droplet; (b) partially wetting (PW) droplet where the liquid partially fills the structure beneath the droplet, and (c) suspended (S) droplet where an air layer fills the structure beneath the droplet[84] (schematics not to scale). Environmental scanning electron microscopy (ESEM)[117-127] images of droplets with the (d) W, (e) PW, and (f) S morphologies on a nanostructured surface (h = 6.1 μm, l = 2 μm, d = 300 nm).Reprinted with permission from reference 84. Copyright 2013, American Society of Mechanical Engineers.

Figure 3 – Effect of structure length scale and nucleation density on emergent droplet morphology. (a) Schematic of a droplet growing within the confines of the structures. The liquid can either grow laterally by filling the adjacent structures or by growing upwards above the structures[54]. Condensed droplet growth observed using ESEM on structured surfaces with (b) Cassie droplets where l = 2 μm and (c) Wenzel droplets where l = 4 μm[55]. Scale bar for (b, c) is 60 μm. Condensation behavior on a microstructured surface (l = 4.5 μm, d = 2 μm, h = 5 μm, and E^* = 0.75 ± 0.04) is shown at a fixed location with a scaled coalescence length of (d) $\langle L \rangle / l$ = 3.54 ± 2.43 (PW droplets) and (e) $\langle L \rangle / l$ = 2.04 ± 0.6 (W droplets)[55]. Scale bar for (d, e) is 50 μm. (f) Regime map characterizing the dominant wetting behavior observed during condensation with coordinates of $\langle L \rangle / l$ and E^*. PW morphologies (red □) emerge at large $\langle L \rangle / l$ and $E^* \lesssim 1$ (shaded region). Wenzel morphologies (blue ○) emerge at low $\langle L \rangle / l$ and/or $E^* \gtrsim 1.55$ Adapted with permission from references 55 (Copyright 2013, American Chemical Society) and 54 (Copyright 2012, Royal Society of Chemistry).

Figure 4 – Effect of droplet morphology on growth rate. Time evolution of the average droplet diameter for (a) PW and (b) S droplets. The S droplet has a slower growth rate than the PW droplet due to poor thermal contact between the base and substrate[67]. (c) PW and S droplet model schematics and thermal resistance diagram showing the liquid-vapor interface (R_i), droplet conduction (R_d), hydrophobic coating (R_{hc}), pillar (R_p), and gap (R_g) thermal resistances[67]. Reprinted with permission from references 67. Copyright 2012, American Chemical Society.

Figure 5 – Droplet departure modes – gravitational shedding versus jumping. Dropwise condensation on a horizontally oriented (a) smooth hydrophobic surface and (b) structured two-tier superhydrophobic surface (with micro pillars visible). Stages 1–3 of the condensation process characterize the initial nucleation, immobile coalescence, and mobile coalescence (jumping droplets), respectively[29]. (c) Coalescing process of two droplets. Upper photos: side-

view imaging of two condensed drops with diameters of 302 and 252 μm during merging; lower: modeled coalescence process[83]. (d) Coalescence-induced transformation and jumping of the merged droplet. Upper photos: side-view images of coalescence-induced droplet jumping; lower: modeled coalescence-induced droplet jumping[83]. Reprinted with permission from references 29 (Copyright 2009, The American Physical Society) and 83 (Copyright 2012, Elsevier).

Figure 6 – Fabricated scalable nanostructured surfaces. FESEM images of a 5 min CuO surface with (a) top view, (b) side view, and (c) micro-goniometer contact angle measurement image ($\theta_a = 169.2 \pm 2.6^o$). The sharp, knife-like CuO structures have characteristic heights, $h \approx 1$ μm, solid fraction, $\varphi \approx 0.023$, and roughness factor, $r \approx 10.47$ (d, e) SEM images of the copper surface structures at a 12 min immersion time[93]. (f) Contact angle measurement on the nanostructured superhydrophobic copper surface (5 μL droplet, $\theta_a = 159 \pm 2^o$)[93]. (g) SEM images of zinc surface (24 h deposition) showing micro-flowers-like structure ($a \approx 12$ μm, $b \approx 25$ μm, $c \approx 10$ μm)[92]. (h) The micro-flower area inside the circle in (g) at large magnification. It shows nano sheets with average thickness 300 nm[92]. (i) Contact angle measurement of a 3 μl water droplet on the ZnO surface. Reprinted with permission from references 47, 93 (Copyright 2013, American Chemical Society), and 92 (Copyright 2010, Elsevier).

Figure 7 – Experimental heat transfer results. (a) Schematic of the planar jumping-droplet thermal diode (not to scale) in forward mode with jumping droplets returning the working fluid from the superhydrophobic condenser to the superhydrophilic evaporator for continuous phase-change heat transfer[100]. (b) Forward thermal conductivity (k_f) versus the average vapor temperature of the thermal diode (T_v)[100]. (c) Schematic showing experimental setup. The tube sample ($D_{OD} = 6.35$ mm, $D_{ID} = 3.56$ mm, $L = 131$ mm) was cooled via chilled water flowing inside the tube at 5 ± 0.1 L/min[47]. (h) Experimental and theoretical steady state condensation coefficient (h_c) as a function of saturated vapor pressure (P_v) for tube surfaces shown in (d) undergoing filmwise, dropwise, flooding ($\tau = 5$, 10, 20, and 45 min), and jumping ($\tau = 10$ min) condensation[47]. Jumping condensation shows the highest condensation HTC for low supersaturations ($S < 1.12$)[47]. Adapted with permission from references 100 (Copyright 2012, American Institute of Physics), and 47 (Copyright 2013, American Chemical Society).

Author biographies and contact information

Nenad Miljkovic

Massachusetts Institute of Technology, Cambridge, MA, USA; tel. 617-981-9247; and email nmiljkov@mit.edu

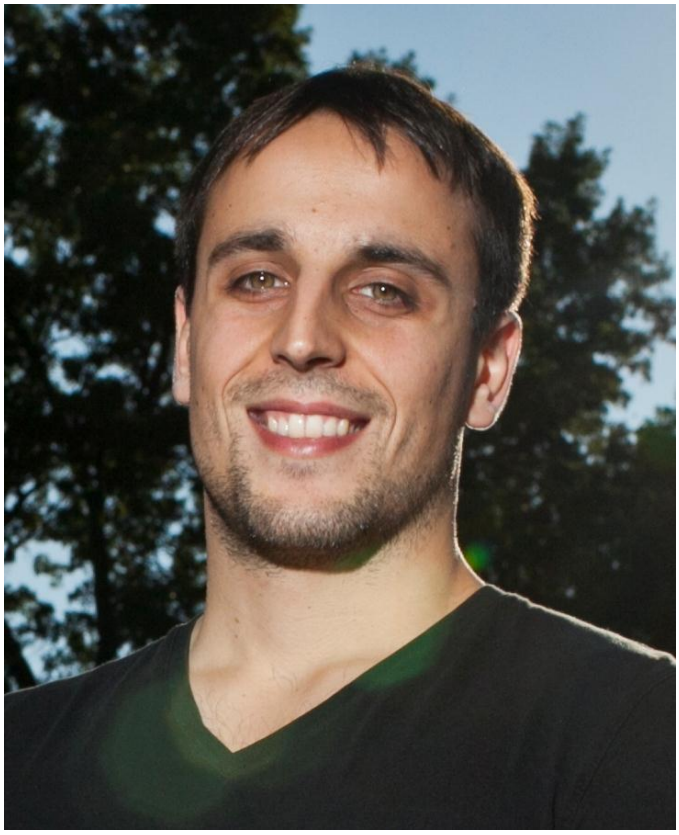

Nenad is a PhD candidate in the Device Research Laboratory in the Department of Mechanical Engineering at the Massachusetts Institute of Technology (MIT). He graduated with a B.A.Sc. degree in mechanical engineering at the University of Waterloo in 2009, and an SM in mechanical engineering at the MIT in 2011. His current research focuses on understanding the fundamental physics of condensation on superhydrophobic surfaces for enhanced condensation heat transfer.

Evelyn N Wang
Massachusetts Institute of Technology, Cambridge, MA, USA; tel. 617-324-3311; and email enwang@mit.edu

Evelyn N. Wang is an Associate Professor in the Mechanical Engineering Department at MIT. She received her BS from MIT in 2000 and MS and PhD from Stanford University in 2001, and 2006, respectively. From 2006-2007, she was a postdoctoral researcher at Bell Laboratories, Alcatel-Lucent. Her research interests include fundamental studies of micro/nanoscale heat and mass transport and the development of efficient thermal management, water desalination, and solar thermal energy systems. Her work has been honored with awards including the 2012 ASME Bergles-Rohsenow Young Investigator Award in Heat Transfer, 2012 Office of Naval Research Young Investigator Award, 2011 Air Force Office of Scientific Research Young Investigator Award, and 2008 DARPA Young Faculty Award.